

# A KNIME-based Analysis of the Zebrafish Photomotor Response Clusters the Phenotypes of 14 Classes of Neuroactive Molecules

*Daniëlle Copmans<sup>1</sup>, Thorsten Meinl<sup>2</sup>, Christian Dietz<sup>3</sup>, Matthijs van Leeuwen<sup>4</sup>, Julia Ortmann<sup>5</sup>,  
Michael R Berthold<sup>3</sup>, Peter AM de Witte<sup>1\*</sup>*

<sup>1</sup>Laboratory for Molecular Biodiscovery, Department of Pharmaceutical and Pharmacological Sciences, KU Leuven, Leuven, Belgium

<sup>2</sup>KNIME.com AG, Zurich, Switzerland

<sup>3</sup>Chair for Bioinformatics and Information Mining, Department of Computer and Information Science, University of Konstanz, Konstanz, Germany

<sup>4</sup>Machine Learning group, Department of Computer Science, KU Leuven, Leuven, Belgium

<sup>5</sup>Department of Bioanalytical Ecotoxicology, Helmholtz Centre for Environmental Research, UFZ, Leipzig, Germany

## **\*Corresponding Author:**

Prof. Dr. Peter A. M. de Witte, Laboratory for Molecular Biodiscovery, Department of Pharmaceutical and Pharmacological Sciences, KU Leuven, Herestraat 49 bus 824, 3000 Leuven, Belgium.

E-mail: peter.dewitte@pharm.kuleuven.be (P.A.M.W.)

Underlying research materials of this study can be requested through the corresponding author.

Keywords: zebrafish, neuroactive drug discovery, photomotor response, data analysis, KNIME

## **ABSTRACT**

Recently, the photomotor response (PMR) of zebrafish embryos was reported as a robust behavior that is useful for high-throughput neuroactive drug discovery and mechanism prediction. Given the complexity of the PMR there is a need for rapid and easy analysis of the behavioral data. In this study, we developed an automated analysis workflow using the KNIME Analytics Platform and made it freely accessible. This workflow allows to simultaneously calculate a behavioral fingerprint for all analyzed compounds and to further process the data. Furthermore, to further characterize the potential of PMR for mechanism prediction, we performed PMR analysis of 767 neuroactive compounds covering 14 different receptor classes using the KNIME workflow. We observed a true positive rate of 25% and a false negative rate of 75% in our screening conditions. Among the true positives, all receptor classes were represented, thereby confirming the utility of the PMR assay to identify a broad range of neuroactive molecules. By hierarchical clustering of the behavioral fingerprints, different phenotypical clusters were observed that suggest the utility of PMR for mechanism prediction for adrenergics, dopaminergics, serotonergics, metabotropic glutamatergics, opioids, and ion channel ligands.

## **INTRODUCTION**

In 2010, the photomotor response (PMR) of zebrafish embryos was reported for the first time as a robust behavior that allows high-throughput neuroactive drug discovery.<sup>1</sup> This study by Kokel and colleagues thoroughly characterized the PMR as a stereotypic series of motor behaviors by zebrafish embryos in response to high intensity light pulses. The potential of a PMR-based behavioral assay was demonstrated in a chemical screen of 14 000 small molecules, identifying hundreds of PMR-modifying hits. As PMR is regulated by multiple neurotransmitter pathways, PMR-modifying molecules are considered to be neuroactive.

Interestingly, PMR behavior was also proven to allow target identification of novel hits by co-clustering of molecules with similar phenotypes and with known mechanism of action (MOA).<sup>1</sup> This characteristic of PMR can have a broad applicability when generating a large reference map of PMR phenotypes of small molecules with known MOA. Then, the MOA of an interesting hit or drug candidate can be predicted by co-clustering and a targeted approach of mechanistic investigation can be done. However, little is known about the predictive value of PMR phenotyping. It has only been characterized in part which neurological pathways can modify the PMR in a robust and distinct manner, and there has been no characterization of pathways that cannot. There has also been no characterization of the rate of false negatives. Thus, there is a need to further characterize the predictive value of the PMR.

PMR is a very complex behavior to analyze and data is generated rapidly by video recording. Motion is recorded as a change in pixels continuously in time for 30 seconds for each well of a 96-well plate. In our set-up, a time frame of 0.067 seconds was used. This implies that for each well, 448 data points are generated in 30 seconds. As replicate wells are used per condition and in case of screening, hundreds up to thousands of molecules are analyzed, an excess of data is rapidly generated. For example, this study resulted in more than 1.5 million data points for the analysis of only 767 compounds. Hence, there is a need for rapid and easy analysis of the behavioral data.

In this study, we developed an automated workflow for PMR analysis using the KNIME Analytics Platform (<http://www.knime.org>).<sup>2</sup> This is an open-source integration platform providing a powerful and flexible workflow system combined with data analytics, visualization, and reporting capabilities. KNIME integrates nodes for machine learning, statistical data analysis, and interfaces to various scripting languages, for example, the statistical programming

language R. KNIME's functionality can be extended with nodes provided via an online repository (the so-called KNIME extensions). Our automated analysis workflow allows simultaneous calculation of a behavioral fingerprint for all analyzed molecules and to further process the data, e.g., by hierarchical clustering. Since the workflow has broad utility for behavioral analysis, it is made freely accessible on the KNIME Public Example Server as 050\_Applications/050021\_PMR Analysis.

Furthermore, to further characterize the potential of the PMR for mechanism prediction, we performed PMR analysis of 767 neuroactive compounds covering 14 different receptor classes (adrenergics, dopaminergics, serotonergics, opioids, sigma ligands, cholinergics, histaminergics, melatonin ligands, ionotropic glutamatergics, metabotropic glutamatergics, GABAergics, purinergics, adenosines, and ion channel ligands) using the KNIME workflow. Our results confirm the utility of the PMR assay to identify a broad range of neuroactive molecules. Moreover, the observations suggest that PMR can be useful for mechanism prediction for adrenergics, dopaminergics, serotonergics, metabotropic glutamatergics, opioids, and ion channel ligands.

## **MATERIALS AND METHODS**

### **Zebrafish maintenance**

Adult zebrafish (*Danio rerio*) stocks of the AB strain (Zebrafish International Resource Center, Oregon, USA) were maintained at 28.0°C, on a 14/10 hour light/dark cycle under standard aquaculture conditions. Fertilized eggs were collected via natural spawning. Embryos and larvae were kept on a 14/10 hour light/dark cycle in embryo medium: 1.5 mM HEPES, pH 7.6, 17.4 mM NaCl, 0.21 mM KCl, 0.12 mM MgSO<sub>4</sub>, and 0.18 mM Ca(NO<sub>3</sub>)<sub>2</sub> in an incubator at 28.0°C. All zebrafish experiments carried out were approved by the Ethics Committee of the

University of Leuven (Ethische Commissie van de KU Leuven, approval number (P101/2010)) and by the Belgian Federal Department of Public Health, Food Safety & Environment (Federale Overheidsdienst Volksgezondheid, Veiligheid van de Voedselketen en Leefmilieu, approval number LA1210199).

### **Compound libraries and compounds**

633 compounds from the Screen-Well Neurotransmitter Library (BML-2810-0100, Enzo Life Sciences), 71 compounds from the Screen-Well Ion Channel Ligand Library (BML-2805-0100, Enzo Life Sciences), 33 selected compounds from the Spectrum Collection library (MicroSource Discovery Systems Inc.), and 30 individually purchased compounds (Sigma-Aldrich, Prestwick) were analyzed by the PMR assay. Positive controls isoproterenol and apomorphine were purchased from Sigma-Aldrich and diazepam was obtained from the pharmacy (Roche, Valium 10 mg/2 ml ampullas).

### **Compound preparation**

Isoproterenol, diazepam, and apomorphine were dissolved in DMSO to 10 mM, 5 mM, 2.5 mM, and 1.25 mM concentrations and 100-fold diluted in the embryo's swimming water (embryo medium) to final concentrations of 100  $\mu$ M, 50  $\mu$ M, 25  $\mu$ M, and 12.5  $\mu$ M with a final solvent concentration of 1% DMSO. 767 compounds were analyzed by the PMR assay at a concentration of 50  $\mu$ M with a final solvent concentration of 0.5% or 1% DMSO. 737 compounds were provided by compound libraries as 10 mM DMSO stocks (water was used as a solvent for DMSO insoluble compounds) and 200-fold diluted in the embryo's swimming water to final concentrations of 50  $\mu$ M (0.5% DMSO). 30 individually purchased compounds were prepared as 5 mM DMSO stocks and 100-fold diluted in the embryo's swimming water to final concentrations of 50  $\mu$ M (1% DMSO). Vehicle (VHC) treated controls were treated

with 0.5% DMSO, 1% DMSO, or water in accordance with the final solvent concentration of the analyzed compounds.

### **Photomotor response assay**

Protocol was adapted from Kokel and colleagues.<sup>1</sup> The photomotor response of zebrafish embryos was investigated by automated behavioral tracking (Zebrabox, Viewpoint) at 30-32 hours post-fertilization (hpf). Zebrafish embryos were placed in a 96-well plate in embryo medium at 27-29 hpf (prim-15 stage), followed by a dark incubation of 3 hours with VHC or compound prior to tracking, including 20 minutes of habituation in the Zebrabox chamber. Concurrent controls were run with each compound to avoid inter-plate variation. Exactly 5 embryos were placed per well to obtain a cumulative photomotor response. Total motion was recorded for 30 seconds at 15 frames per second (fps) in fully dark conditions with a high intensity light pulse (5.2 mW/cm<sup>2</sup>, 38 000 lux) given at 10 and 20 seconds lasting one second. Raw data of total movement per well was used and is defined as the sum of all image pixel changes detected during the time interval of 0.067 seconds, corresponding to one frame. Total motion was plotted in function of time and average motion was plotted per time period. The PMR was divided in 8 time periods. The so-called pre-stimulus phase, at which embryos show basal activity, was considered as 1 time period (PRE; seconds 0-10). The latency phase, which occurs immediately after the first light stimulus, was considered as 1 period (L; seconds 10-11). The excitatory phase, at which embryos shake vigorously, was divided in three periods (E1; seconds 11-13, E2; seconds 13-16, E3; seconds 16-20). Finally, the refractory phase, at which embryos show a lower than basal activity, is triggered by the second light stimulus and was divided in three periods as well (R1; seconds 20-22, R2; seconds 22-25, R3; seconds 25-30). For control experiments with isoproterenol, diazepam, and apomorphine, data were pooled from three independent experiments with 4 to 6 replicate wells per condition. For screening of

neuroactive molecules, data were pooled from 3 or 6 replicate wells per molecule. Replicate wells were scattered over the 96-well plate. The PMR assay was standardized for temperature at 28°C, including habituation and behavioral tracking in the Zebrabox, which was placed in an incubator for temperature control. Automated behavioral tracking was standardized for light intensity by the usage of only the 30 central wells of a 96-well plate, ensuring identical light intensity regardless of the position.

### **Microscopic evaluation of toxicity**

The PMR assay was immediately followed by visual evaluation of the embryos by a light microscope to assess toxicity of pharmacological treatment. Overall morphology, heartbeat, and touch response was investigated. Overall morphology was considered as normal in case of a normal appearance. Overall morphology was considered as abnormal, in case of signs of necrosis, which was especially seen at the tip of the tail. We did not encounter other morphological abnormalities like edema or developmental defects. The heartbeat was considered as normal, reduced, or absent. The behavioral response of embryos to touch was investigated by touching the chorion of the embryo at the site of the yolk with a bold needle. Touch response was considered as normal (including hyperactivity), reduced, or absent. Compounds were scored as normal (N) if exposed embryos had a normal morphology, heartbeat, and touch response. Compounds were scored as sedative (S) if exposed embryos had a normal morphology, normal or reduced heartbeat, and a reduced or absent touch response. Compounds were scored as toxic (T) if exposed embryos had an abnormal morphology, or an absent touch response with absence of heartbeat.

### **Behavioral fingerprints**

Behavioral fingerprints were calculated by an automated workflow using KNIME Analytics Platform 2.11.3. A behavioral fingerprint represents the embryonic motion during the 8 PMR periods by subsequent numeric values. Each period was described by the first (25% of motion, Q1) and third quantile (75% of motion, Q3), giving a total of 16 numeric values. For comparison with VHC treated embryos, pseudo Z-scores were calculated for each log-transformed quantile by the following formula:

$$\text{pseudo Z - score} = \frac{\mu_{\text{treatment}} - \mu_{\text{control}}}{\sigma_{\text{control}}}$$

The mean value ( $\mu$ ) of the control condition is subtracted from the mean value of the treatment condition and the result is divided by the standard deviation ( $\sigma$ ) of the control condition to obtain the pseudo Z-score. The behavioral fingerprints consist of 16 subsequent pseudo Z-scores, calculated from the Q1 and Q3 from each PMR period. The definition and calculation of behavioral fingerprints or barcodes is adapted from Kokel and colleagues.<sup>1,3</sup>

### **KNIME Analytics Platform**

Supplemental Figure S1 shows the main window of the KNIME Analytics Platform. On the left the “KNIME Explorer” shows the available workflows. The “Node Repository” contains the available nodes. In the center an open workflow is shown. A description of the selected node is given at the right of the window. The “Console” is seen at the bottom which gives details about warnings and errors that occurred during workflow execution (**Suppl. Fig. S1**).

A KNIME workflow is composed of multiple nodes that are connected by ports. Data is passed along the connections between ports in a table structure with columns (each having a certain type) and rows. The parameters of nodes and their documentation are available via a configuration dialog. More complex workflows, such as the one we developed and describe below, contain also loops and switches. Loops allow applying the same series of nodes to

multiple input files one at a time and switches allow executing only certain branches of the workflow based on user-defined conditions. To further structure a workflow, KNIME provides the so-called meta-nodes to group a collection of nodes. Grouping into meta-nodes can be used to hide a complex series of nodes and instead provide a high-level view on the data flow.

## RESULTS

### PMR analysis of positive controls isoproterenol, diazepam, and apomorphine

To validate our optimized PMR assay, three drugs with known PMR-modifying effects were analyzed, i.e., isoproterenol, diazepam, and apomorphine. These drugs were earlier shown by Kokel and colleagues to cause excitation, inhibition, and latency of the excitatory phase, respectively.<sup>1</sup>

Embryos incubated for 3 hours with 100  $\mu$ M isoproterenol demonstrated an overall excitation of the photomotor response in comparison with VHC treated controls. This increase in motion was observed to be significant at the pre-stimulus phase ( $p < 0.01$ ), latency phase ( $p < 0.05$ ), and first ( $p < 0.001$ ) and second ( $p < 0.05$ ) excitation period (**Fig. 1A, B**). Embryos incubated for 3 hours with 100  $\mu$ M diazepam demonstrated an overall inhibition of the PMR in comparison with VHC treated controls. This decrease in motion was observed to be significant at the pre-stimulus phase ( $p < 0.001$ ), latency phase ( $p < 0.01$ ), and first ( $p < 0.001$ ) and second ( $p < 0.001$ ) excitation period (**Fig. 1C, D**). Finally, embryos incubated for 3 hours with 100  $\mu$ M apomorphine demonstrated a complex altered PMR in comparison to VHC treated embryos. The PRE motion was lowered, no difference was seen in the E1 period, and a significant increase in motion was observed for the E2 ( $p < 0.001$ ), E3 ( $p < 0.001$ ), and R1 ( $p < 0.01$ ) period. These latter observations were due to the occurrence of a second excitation peak, delayed to the incidence of the first excitation peak. This excitation peak only slowly passed in comparison

with the normal excitation peak of control embryos (**Fig. 1E, F**). Concentration dependency was observed for all phenotypes (**Fig. 1G**). Taken together, these observations suggest that our PMR assay can detect PMR-modifying effects very similarly to those reported by Kokel and colleagues.

### **Generation of an automated KNIME workflow for large-scale PMR analysis**

For our large-scale PMR analysis of neuroactive molecules, behavioral analysis had to be rapid, easy, and automated. Therefore, a KNIME workflow was built to analyze the data recorded by the Zebrafish. It computes the pseudo Z-scores and behavioral fingerprints for each molecule, and finally performs hierarchical clustering of the pseudo Z-scores and generates a dendrogram. The workflow is rather complex, as it performs all steps from reading the raw data until the final dendrogram. In order to make it more readable it has therefore been divided into several sections using the meta-node concept mentioned in the materials and methods. The workflow is shown in Figure 2. For reasons of space we will only highlight the important parts. The complete workflow, including inline comments, can be downloaded from KNIME's Public Example Server directly from within KNIME (login via the entry in the "KNIME Explorer" view).

The workflow requires two types of input. The first input is the raw data, which consists of several CSV files (one per 96-well plate) containing raw measurements for all wells on the plate over the 30 seconds interval (about 28 000 rows per file). The data is divided into three columns: time, well ID (e.g., "c1", "c2"), and the embryonic motion measurement. The workflow iterates over all files in the experiment's directory and computes the behavioral fingerprint for each molecule (see below). The second input is a file that contains a mapping between the plates/wells and the treatment in each well (referred to as substance in the workflow), e.g., VHC

or a certain molecule. Additionally it may contain manual annotations, indicating whether a well should be ignored in the further analysis, e.g., because the well was empty or no treatment was added.

Computation of the behavioral fingerprints inside the “Calculate fingerprint” meta-node works as follows (**Fig. 3A**). First the raw input data is transformed from the three-column structure described above into a table with a column for each well and a row for each time point (“Data Transformation” meta-node). The values in the cells are the measurements. The “Unify Domains” meta-node ensures that the y-axes in the lines plots have the same scales and can therefore be directly compared. Figure 3B shows some plots generated by the “Line Plots” meta-node. The Numeric Binner assigns names to the time intervals (“segments”) as described above (e.g., “L”, “E1”, “R1”). The “Group Loop” iterates over the measurements in each of the segments separately. For each well/substance in each segment, we compute the 25% and 75% quantiles (Q1 and Q3, respectively) and use the logarithms of these values in subsequent steps (“Calculate Quartiles” meta-node). Figure 3C shows parts of the resulting table for segment “R3”. Finally, we compute the pseudo Z-scores based on the quartiles of the controls and the molecules, and transform the structure to obtain a row for each segment and a pseudo Z-score (Q1 and Q3) with the corresponding values for each molecule in the columns (**Fig. 3D**). This is the result of the outermost loop, which completes the computation of all values for all plates. Note also the “Check bad measurements” meta-node in the center of Figure 3A. This node provides an extra internal control to avoid the analysis of a plate when multiple control wells are ignored due to an error, e.g., a software error or manual error. It checks the manual annotations for all wells and if such plate occurs, it fails and will stop execution of the remaining workflow.

The next step is to remove all columns/molecules with pseudo Z-scores below a certain threshold. The threshold can easily be set by the user via the configuration dialog of the “Filter substances” meta-node, without having to know the other details of the filtering.

In the bottom part of the main workflow (**Fig. 2**) we first transpose the table so that each molecule is in a row and the pseudo Z-scores for the segments are in the columns. Next, we remove the segment ‘IGNORE’ that represents seconds just before and after the 30 second PMR period that are not taken into account. Then we compute a distance matrix (Euclidean distance) using the pseudo Z-scores as dimensions and perform hierarchical clustering with complete linkage. The final result is a dendrogram, including a heatmap, as shown in Figure 4 and discussed in the next sections.

### **PMR analysis of 14 classes of neuroactive molecules**

A systematic analysis was done of 767 neuroactive molecules covering 14 different receptor classes (adrenergics, dopaminergics, serotonergics, opioids, sigma ligands, cholinergics, histaminergics, melatonin ligands, ionotropic glutamatergics, metabotropic glutamatergics, GABAergics, purinergics, adenosines, and ion channel ligands) to further characterize the neurological pathways that can alter PMR. Embryos were incubated either with vehicle (0.5 or 1% DMSO) or with 50  $\mu\text{M}$  of a certain molecule (final solvent concentration of 0.5 or 1% DMSO) for 3 hours prior to PMR analysis. PMR analysis was followed by microscopic evaluation of embryo morphology, heartbeat, and touch response, to assess toxicity of pharmacological treatment. A low rate of sedative (3.4%) and toxic (2.2%) compounds was observed, suggesting that 50  $\mu\text{M}$  of most neuroactive compounds is well tolerated by zebrafish embryos during an acute exposure (**Table 1**).

A PMR positive molecule was defined as a molecule that modifies the photomotor response such that its behavioral fingerprint contains at least one pseudo Z-score with an absolute value exceeding 3. At this critical value, 195 molecules were observed to be PMR positive, giving a true positive rate of 25.4% and a false negative rate of 74.6%. Thus, 25.4% of known neuroactive molecules alter PMR sufficiently at the analyzed concentration to be identified as neuroactive by the PMR assay. At a lower critical value of 2, 324 molecules were PMR positive, giving a true positive rate of 42.2% and a false negative rate of 57.8%. This lower stringency allows the detection of more than 40% of the neuroactive molecules at 50  $\mu$ M. At a higher critical value of 5, 117 molecules were still observed to be positive, giving a true positive rate of 15.3% and a false negative rate of 84.7% (**Table 1**). These PMR positives alter the PMR so much that a difference in motion of at least 5 times the standard deviation of the control is seen. For further analysis the critical value of 3 was taken to consider only neuroactive molecules that alter PMR in a robust manner.

Among PMR positive molecules, all neurological pathways are represented as molecules from all receptor classes were included. This observation confirms the utility of PMR to detect a broad range of neuroactive molecules and suggests the involvement of these pathways in PMR regulation.

### **Hierarchical clustering of PMR positive molecules**

To characterize the classes of neuroactive molecules that can induce a distinct PMR phenotype, hierarchical clustering of behavioral fingerprints of the 195 PMR positive molecules was done (**Fig. 4**). A cluster was considered to be enriched with molecules from a certain neurological pathway if more than one third of the molecules belongs to a single receptor class and the cluster has a minimum size of 7 fingerprints. This was determined in a top-down approach evaluating

the 30 most distinct clusters of the heatmap as indicated by the workflow. 8 clusters were observed to be enriched with a certain class of molecules. These clusters are indicated by numbers 1-8 in Figure 4.

Cluster 1 is enriched with behavioral fingerprints from opioids. 5 out of 7 molecules are opioid receptor ligands. These show a higher activity in the E1 and E2 period in comparison to control behavior and a reduced activity in periods E3, R1, R2, and R3 (cluster 1; **Suppl. Fig. S2**).

Cluster 2 is enriched with ligands from metabotropic glutamatergic receptors. 4 out of 10 molecules belong to this class of receptors, 3 of them are receptor agonists. These molecules show a behavioral fingerprint with decreased activity mainly in periods E2 and E3, but also in R1-3 (cluster 2; **Suppl. Fig. S2**).

Cluster 4 is also enriched with ligands from metabotropic glutamatergic receptors, but all are receptor antagonists. 4 out of 9 molecules belong to this class of receptors and show a reduced activity especially in the PRE, E1, and E2 period in comparison to controls (cluster 4; **Suppl. Fig. S2**). 3 of these molecules have the mGlu5 receptor as target.

Cluster 3 is enriched with ligands from adrenergic receptors. 10 out of 23 molecules belong to this class of receptors, 8 of them are receptor agonists and 7 molecules are  $\alpha$  receptor ligands. They show a behavioral fingerprint with an overall increased activity in comparison to controls (cluster 3; **Suppl. Fig. S2**).

Cluster 5 is enriched with ligands from dopaminergic receptors. 6 out of 8 molecules belong to this receptor class, 5 of them are receptor agonists. Their behavioral fingerprints show a decreased activity especially in the PRE and E1 phase (cluster 5; **Suppl. Fig. S2**).

Cluster 8 is also enriched with ligands from dopaminergic receptors. 11 out of 26 molecules belong to this class of receptors, both agonists and antagonists. 6 of them are D4 receptor ligands. Their behavioral fingerprints show also a decreased activity in the PRE phase, but in comparison to cluster 5, the activity in the E1 period is much more decreased (cluster 8; **Suppl. Fig. S2**).

Cluster 6 is enriched with behavioral

fingerprints from different types of ion channel ligands. 12 out of 33 molecules belong to this type of ligands and 8 of them act on calcium channels. Their behavioral fingerprints show a decreased motion during the E1 and E2 period and a moderate decrease or increase in motion in periods E3-R3 (cluster 6; **Suppl. Fig. S2**). Finally, cluster 7 is part of cluster 6. This smaller cluster is also enriched with ligands from serotonergic receptors. 5 out of 13 molecules belong to this receptor class. Their behavioral fingerprints are very similar to those from cluster 6, but this subset shows a more decreased activity in the E1 and E2 period (cluster 7; **Suppl. Fig. S2**).

In summary, ligands from the following classes of receptors were observed to induce a distinct PMR phenotype: adrenergics, dopaminergics, serotonergics, metabotropic glutamatergics, opioids, and ion channel ligands. This means that sigma ligands, cholinergics, histaminergics, melatonin ligands, ionotropic glutamatergics, GABAergics, purinergics, and adenosines seem to fail to induce a distinct PMR phenotype despite of their strong PMR-modifying effects. This data suggests that PMR is useful for mechanism prediction only within the above first mentioned neurological pathways.

## **DISCUSSION**

With this study a systematic PMR analysis was done of the different neurological pathways by analysis of 767 ligands that cover 14 receptor classes. Our results confirm the utility of the PMR assay to identify a broad range of neuroactive molecules, as was demonstrated by Kokel and colleagues.<sup>1</sup> The use of the PMR for mechanism prediction was further investigated and is suggested to be limited to adrenergics, dopaminergics, serotonergics, metabotropic glutamatergics, opioids, and ion channel ligands. Our data thereby confirms the study by Kokel and colleagues who also reported phenotypical clusters for adrenergic and dopaminergic agonists.<sup>1</sup> Furthermore, we expand their findings with the report of distinct phenotypical

clusters for serotonergics, metabotropic glutamatergics, opioids, and ion channel ligands. In contrast to the study by Kokel we did not identify a cluster enriched with adenosine receptor antagonists. This is likely due to differences in protocol, e.g., incubation time (3 hours versus 2-10 hours), but can also be due to the more sensitive detection of embryonic motion by our set-up (detection of motion in the entire well versus detection of motion at 6 lines covering the well).

The identification of phenotypic clusters from adrenergics, dopaminergics, serotonergics, metabotropic glutamatergics, opioids, and ion channel ligands suggests that within these classes new molecules can be identified and the mechanism can be predicted by phenotypic similarity. This allows the use of PMR not only to screen for neuroactivity in general, but also to screen for a certain class of ligands, indicating their potential therapeutic use. Our data suggests that this is not possible for all neurological pathways, but limited to the receptor classes mentioned above. Concerning the detail of mechanism prediction, an indication for agonistic or antagonistic activity is clear in 4 of the 8 clusters, but an indication for a specific target or receptor is not so common. In our data set only 4 targets were highly present in their respective clusters, i.e., the mGlu5 receptor,  $\alpha$  receptor, calcium channel, and the D4 receptor. This is not surprising as the annotated activity of a molecule will not always reflect its activity on the zebrafish target. This is due to possible differences between zebrafish and human receptors and is referred to as the zebrafish annotation problem.<sup>4</sup> Nevertheless, PMR phenotyping can be used for target prediction when screening for molecules without a predefined target. This is suggested by our data and was already demonstrated by Kokel and colleagues who identified novel acetylcholinesterase inhibitors by phenotypic similarity.<sup>1</sup>

The absence of phenotypic clusters from the other classes of ligands is due to the absence of distinct PMR phenotypes for each class and can have multiple causes. First, ligands from different classes can (in)directly affect the same PMR-regulating neurological pathway or affect different neurological pathways with a similar PMR-modifying effect. Second, there can be a large variation between ligands from the same receptor class in terms of conservation of the drug target in zebrafish, optimal test concentration, or drug absorption which all can result in different PMR phenotypes. Third, as many neuroactive ligands have multiple targets it is possible that these ligands do not induce a similar PMR phenotype within a certain class.

Furthermore, we observed a high false negative rate for PMR analysis at the analyzed concentration of 50  $\mu\text{M}$  and after an acute exposure of 3 hours. Analysis of multiple concentrations and exposure times will increase the number of true positives, but this will also largely reduce the throughput. Moreover, as many neuroactive drugs act on multiple targets it can be expected to detect less specific behavioral fingerprints when analyzing compounds at high concentrations. Therefore, ideally, a concentration-response analysis should be performed for each compound to allow improved clustering of the fingerprints based on cross-concentration behavioral similarities within receptor classes. Such an approach would not only reduce the false negative rate, but could also improve phenotype-based mechanism predication. Besides the analysis of compounds at a single concentration and exposure time, other causes for the observation of false negatives in this study could be: malabsorption of the drug, failure of the immature metabolism to activate prodrugs, absence of the functional target in zebrafish or in the immature brain, or the drug target is not involved in PMR regulation.

For improved understanding of our results it is important to know which neurological pathways are present in the immature brain of the zebrafish embryo. The PMR occurs between 30 and 40

hpf, while the light-evoked refractory phase is already observed from 27 hpf onwards.<sup>5</sup> At these stages primary neurogenesis is ongoing until 48 hpf when secondary neurogenesis initiates. Primary neurogenesis involves the transient establishment of an early sensorimotor circuit that allows motor behaviors. These neurons were reported to include glutamatergic, GABA-ergic, cholinergic, and glycinergic neurotransmission at 24 hpf.<sup>6-8</sup> Furthermore, spatiotemporal expression of aminergic innervation in the developing zebrafish embryo demonstrated dopaminergic, (nor)adrenergic, and serotonergic neurotransmission at 24 hpf. Adrenergic or noradrenergic neurons were observed in the hindbrain in the developing locus coeruleus and by 36 hpf as well in the medulla oblongata. Dopaminergic neurons were also observed in the locus coeruleus and furthermore in the posterior tuberculum that is localized in the diencephalon (forebrain). Serotonergic neurons were also observed in the posterior tuberculum and by 32 hpf in the spinal cord as well.<sup>9,10</sup> Finally, spatiotemporal expression of the zebrafish opioid receptors shows a wide distribution in the central nervous system at 24 and 48 hpf.<sup>11,12</sup> The early establishment of the main neurotransmission systems before and by the time of PMR initiation is in accordance with the phenotypical clusters we could detect. Moreover, the early aminergic innervation of the spinal cord by the hindbrain, which is described in a study by McLean and Fetcho<sup>9</sup>, is in line with the sudden shift in motor behavior from low-frequent touch responses until 26 hpf to high-frequent swimming from 28 hpf onwards.<sup>8</sup> This swimming behavior is involved in the PMR and was shown to be driven by photosensitive hindbrain neurons.<sup>5</sup>

Expression studies have also demonstrated the early presence of adenosine<sup>13</sup>, purinergic<sup>14,15</sup>, and melatonin<sup>16</sup> receptors in the central nervous system of the developing zebrafish embryo at 24 hpf. This is in line with the identification of multiple PMR positive molecules from these receptor classes. We also identified PMR positive molecules that act through histamine or sigma

receptors, suggesting their functionality at these early stages. The presence of these receptors in the central nervous system at 30 hpf has not yet been reported, to our knowledge, as only few studies have been done that did not include spatiotemporal investigations at this early stage.<sup>17-</sup>

19

Furthermore, with this study a KNIME workflow was built to analyze behavioral data in a rapid and easy manner. The workflow is designed to calculate behavioral fingerprints for hundreds up to thousands of treatments at the same time, and finally to hierarchically cluster these fingerprints. This workflow enables everyone, without the need for programming skills or IT experience, to analyze behavioral data. Parameters can easily be changed through the configuration button of each node, e.g., the type of distance measure, the type of linkage, and the critical pseudo Z-score value can be changed. Moreover, the workflow is designed such that nodes can easily be removed, added or changed to alter the type of analysis.

Finally, in this study we focused on the applicability of the photomotor response, which is a non-visual light-driven behavioral response. Other types of behavioral responses to neuronal stimuli can also be used for neuroactive drug discovery, e.g., visual light-driven responses, auditory responses. One example is the automated rest/wake behavioral assay that was reported by Rihel and colleagues for phenotype-based target prediction and drug discovery.<sup>20</sup> The challenge becomes to correlate these different types of neuronal responses in drug screening strategies. One possibility is to generate a battery of different behavioral assays and to combine the results as different bars within a descriptive barcode. Such an approach allows a more detailed level of phenotypic description and is expected to improve drug discovery and target prediction. This principle is referred to as behavioral barcoding and has been previously described.<sup>3</sup>

## FUNDING

Matthijs van Leeuwen is supported by a Postdoctoral Fellowship of the Research Foundation Flanders (FWO).

## REFERENCES

1. Kokel, D.; Bryan, J.; Laggner, C.; et al. Rapid Behavior-Based Identification of Neuroactive Small Molecules in the Zebrafish. *Nat. Chem. Biol.* **2010**, *6*, 231–237.
2. Berthold, M. R.; Cebron, N.; Dill, F.; et al. KNIME - The Konstanz Information Miner. *SIGKDD Explor.* **2009**, *11*, 26–31.
3. Kokel, D.; Rennekamp, A. J.; Shah, A. H.; et al. Behavioral Barcoding in the Cloud: Embracing Data-Intensive Digital Phenotyping in Neuropharmacology. *Trends Biotechnol.* **2012**, *30*, 421–425.
4. Rihel, J.; Schier, A. Behavioral Screening for Neuroactive Drugs in Zebrafish. *Dev. Neurobiol.* **2012**, *72*, 373–385.
5. Kokel, D.; Dunn, T. W.; Ahrens, M. B.; et al. Identification of Nonvisual Photomotor Response Cells in the Vertebrate Hindbrain. *J. Neurosci.* **2013**, *33*, 3834–43.
6. Wullimann, M. F. Secondary Neurogenesis and Telencephalic Organization in Zebrafish and Mice: A Brief Review. *Integr. Zool.* **2009**, *4*, 123–133.
7. Higashijima, S. I.; Schaefer, M.; Fetcho, J. R. Neurotransmitter Properties of Spinal Interneurons in Embryonic and Larval Zebrafish. *J. Comp. Neurol.* **2004**, *480*, 19–37.
8. Saint-Amant, L. Development of Motor Rhythms in Zebrafish Embryos. In *Progress in Brain Research*; Elsevier B.V., 2010; Vol. 187, pp. 47–61.
9. McLean, D. L.; Fetcho, J. R. Ontogeny and Innervation Patterns of Dopaminergic, Noradrenergic, and Serotonergic Neurons in Larval Zebrafish. *J. Comp. Neurol.* **2004**, *480*, 38–56.
10. Holzschuh, J.; Ryu, S.; Aberger, F.; et al. Dopamine Transporter Expression Distinguishes Dopaminergic Neurons from Other Catecholaminergic Neurons in the Developing Zebrafish Embryo. *Mech. Dev.* **2001**, *101*, 237–243.
11. Sanchez-Simon, F. M.; Rodriguez, R. E. Developmental Expression and Distribution of Opioid Receptors in Zebrafish. *Neuroscience* **2008**, *151*, 129–137.

12. Gonzalez-Nunez, V.; Rodríguez, R. E. The Zebrafish: A Model to Study the Endogenous Mechanisms of Pain. *ILAR J.* **2009**, *50*, 373–386.
13. Boehmler, W.; Petko, J.; Woll, M.; et al. Identification of Zebrafish A2 Adenosine Receptors and Expression in Developing Embryos. *Gene Expr Patterns* **2009**, *9*, 144–151.
14. Norton, W.; Rohr, K.; Burnstock, G. Embryonic Expression of a P2X3 Receptor Encoding Gene in Zebrafish. *Mech. Dev.* **2000**, *99*, 149–152.
15. Kucenas, S.; Li, Z.; Cox, J. a.; et al. Molecular Characterization of the Zebrafish P2X Receptor Subunit Gene Family. *Neuroscience* **2003**, *121*, 935–945.
16. Danilova, N.; Krupnik, V. E.; Sugden, D.; et al. Melatonin Stimulates Cell Proliferation in Zebrafish Embryo and Accelerates Its Development. *FASEB J.* **2004**, *18*, 751–753.
17. Eriksson, K. S.; Peitsaro, N.; Karlstedt, K.; et al. Development of the Histaminergic Neurons and Expression of Histidine Decarboxylase mRNA in the Zebrafish Brain in the Absence of All Peripheral Histaminergic Systems. *Eur. J. Neurosci.* **1998**, *10*, 3799–3812.
18. Peitsaro, N.; Sundvik, M.; Anichtchik, O. V.; et al. Identification of Zebrafish Histamine H1, H2 and H3 Receptors and Effects of Histaminergic Ligands on Behavior. *Biochem. Pharmacol.* **2007**, *73*, 1205–1214.
19. Moritz, C.; Berardi, F.; Abate, C.; et al. Live Imaging Reveals a New Role for the Sigma-1 ( $\sigma$ 1) Receptor in Allowing Microglia to Leave Brain Injuries. *Neurosci. Lett.* **2015**, *591*, 13–18.
20. Rihel, J.; Prober, D. a.; Arvanites, A.; et al. Zebrafish Behavioral Profiling Links Drugs to Biological Targets and Rest/wake Regulation. *Science.* **2010**, *327*, 348–351.

## TABLE

**Table 1.** PMR analysis of neuroactive compounds

	Number of molecules	Rate (%)	
Total	767		
Normal (N)	724	94.4	
Sedative (S)	26	3.4	
Toxic (T)	17	2.2	toxicity rate
Pseudo Z-score $\geq  2 $			
positives	324	42.2	true positive rate
negatives	443	57.8	false negative rate
Pseudo Z-score $\geq  3 $			
positives	195	25.4	true positive rate
negatives	572	74.6	false negative rate
Pseudo Z-score $\geq  5 $			
positives	117	15.3	true positive rate
negatives	650	84.7	false negative rate

## LEGENDS

**Figure 1.** PMR of 30-32 hpf zebrafish embryos incubated with positive controls isoproterenol, diazepam, and apomorphine. Embryos were treated for 3 hours with vehicle (VHC) or 100  $\mu$ M of drug. **(A, C, E)** Total motion of the embryos as function of time. **(B, D, F)** Mean motion of the embryos as function of 8 PMR periods. **(G)** Mean behavioral fingerprints of embryos treated with 12.5, 25, 50, and 100  $\mu$ M of isoproterenol, diazepam, and apomorphine, respectively. **(A-F)** Data are expressed as mean  $\pm$ SEM. Statistical analysis was done by two-way ANOVA (GraphPad Prism 5). Significance levels: \*  $p < 0.05$ ; \*\*  $p < 0.01$ ; \*\*\*  $p < 0.001$ .

**Figure 2.** KNIME workflow for PMR analysis. The workflow structure is using meta-nodes in order to make it more readable and easier to maintain.

**Figure 3.** A detailed view of the meta-node that computes the behavioral fingerprints. **(A)** Inside view of the meta-node 'Calculate fingerprint for plate'. The meta-node is again divided into several nested meta-nodes. **(B)** Result table of the meta-node 'Line Plots'. Line plots show

the embryonic motion in time in a certain well. (C) Result table of the meta-node 'Calculate Quartiles' showing some computed quantiles for segment R3. (D) Final result table showing the pseudo Z-scores for tested molecules.

**Figure 4.** Hierarchical clustering of PMR positive molecules. Behavioral fingerprints of PMR positive molecules were clustered by complete linkage of the distance matrix (Euclidean distance). (A) Heatmap and dendrogram is shown. Numbers 1-8 indicate clusters that are enriched with molecules from a single receptor class. (B) Color scales of the heatmap are given for the first (Q1) and third quantile (Q3) for all PMR periods. PRE, pre-stimulus phase; L, latency phase; E1, excitatory period 1; E2, excitatory period 2; E3, excitatory period 3; R1, refractory period 1; R2, refractory period 2; R3, refractory period 3.

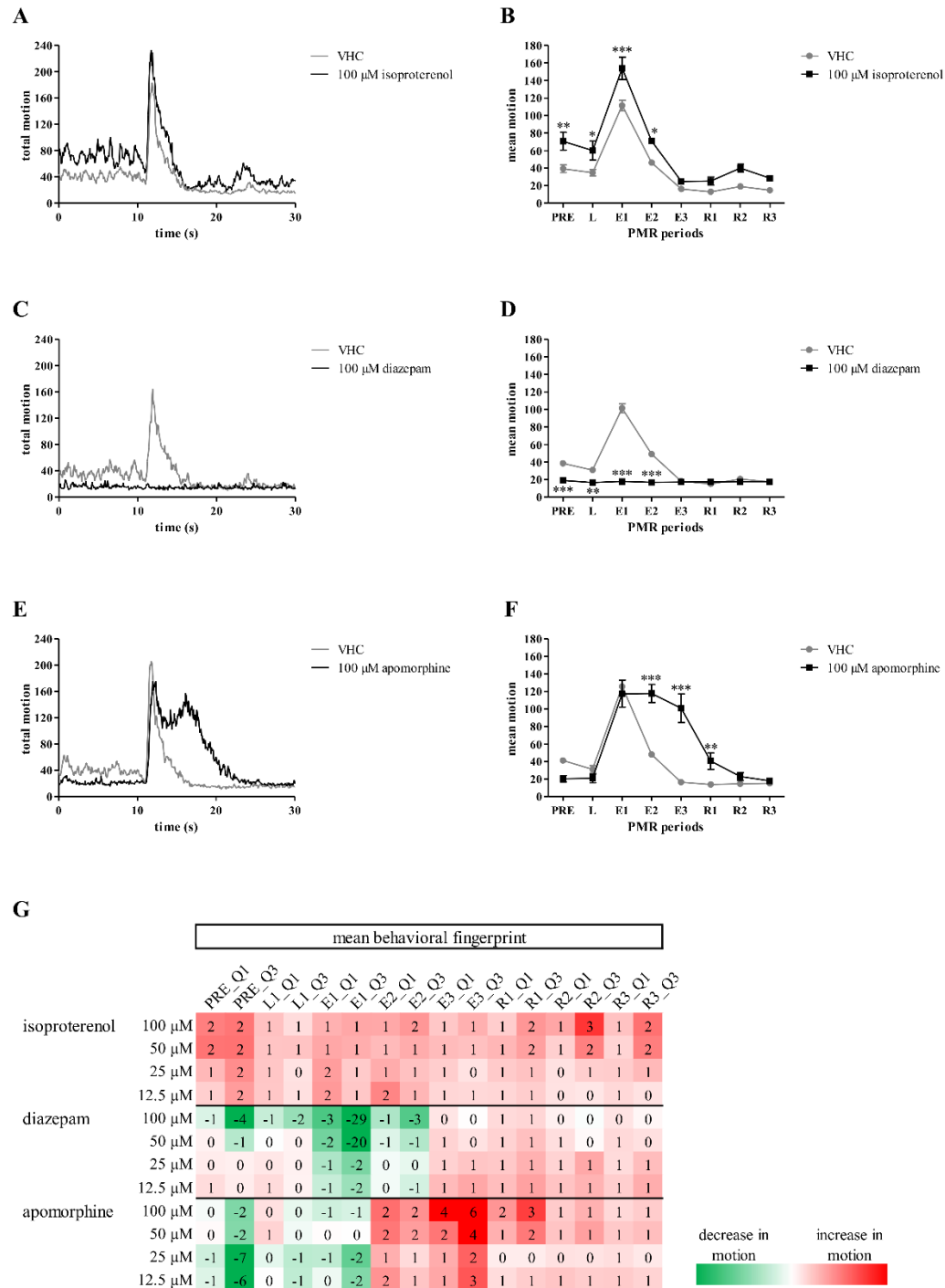


Figure 1

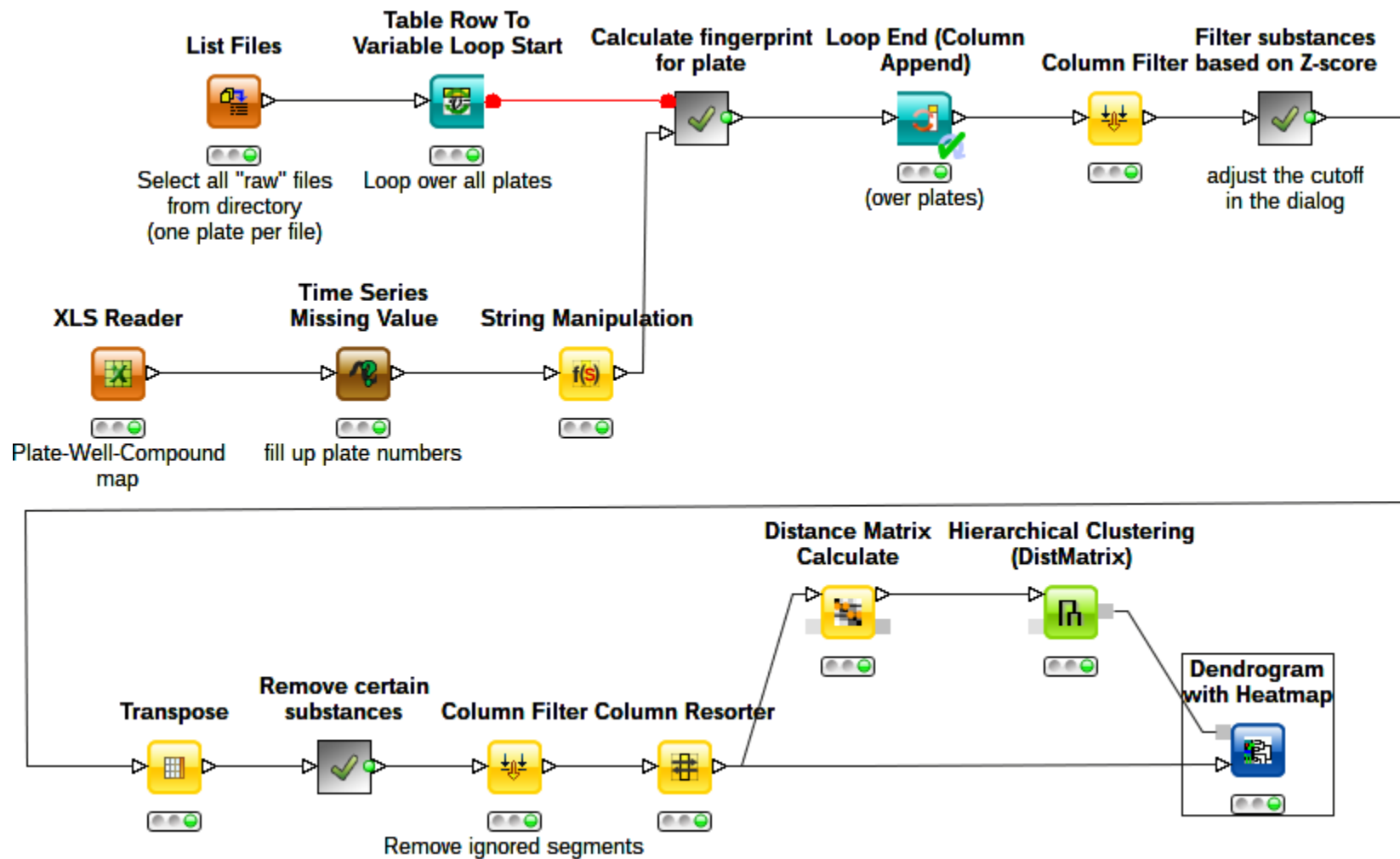
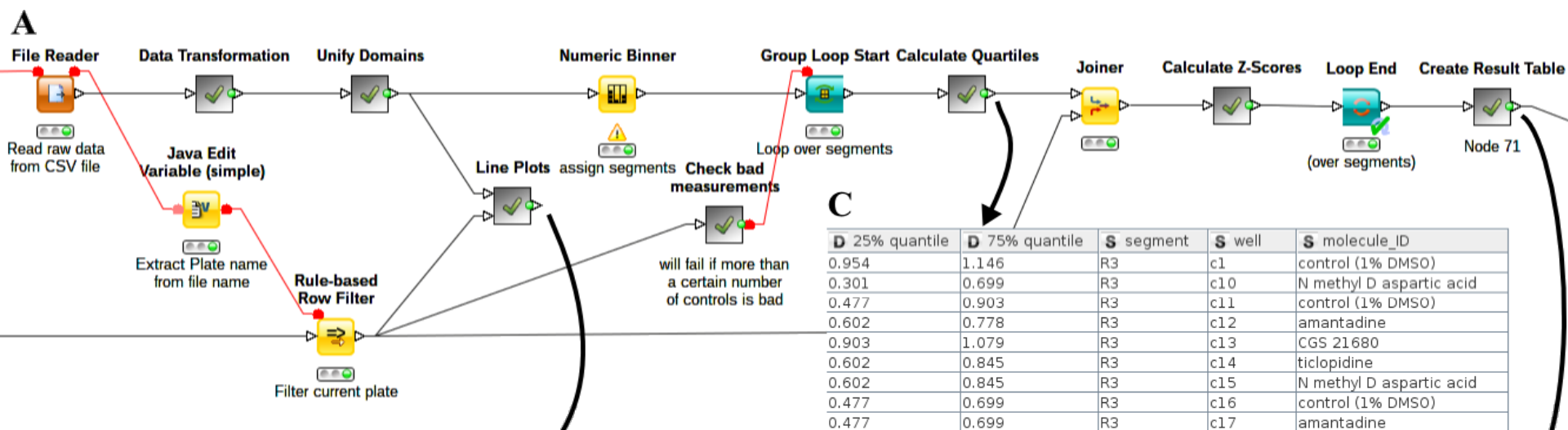
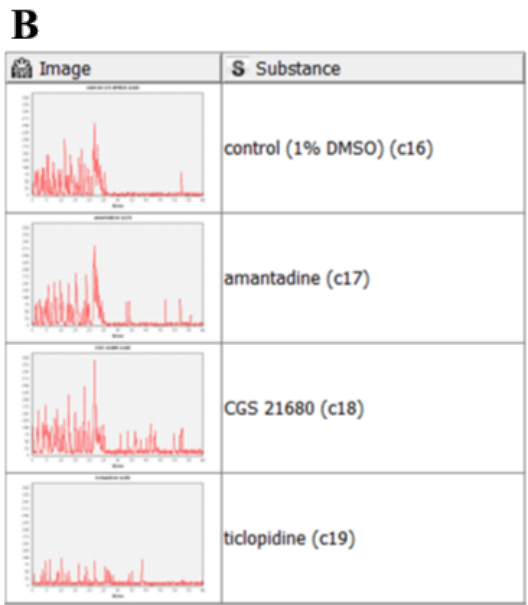


Figure 2



**C**

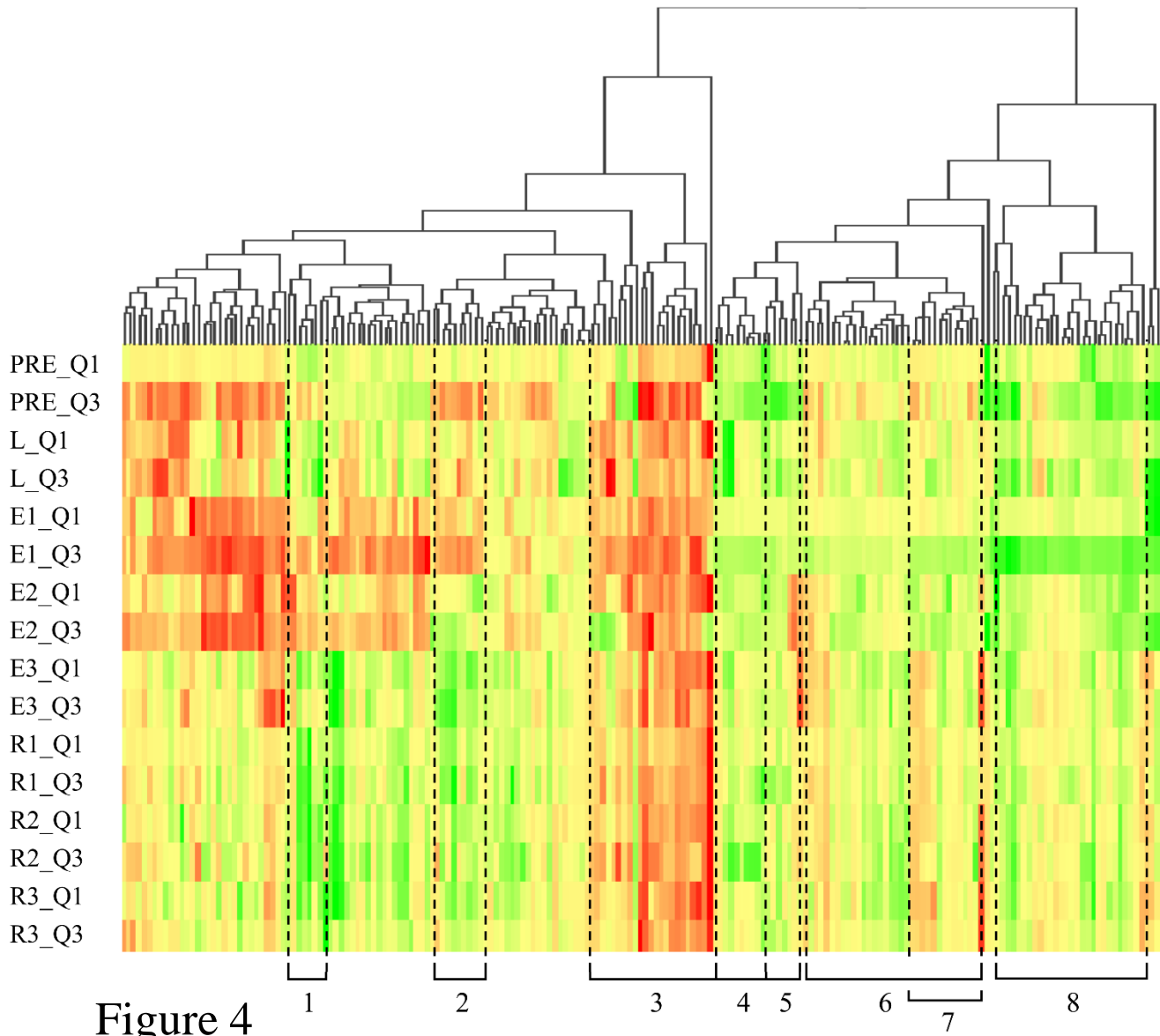
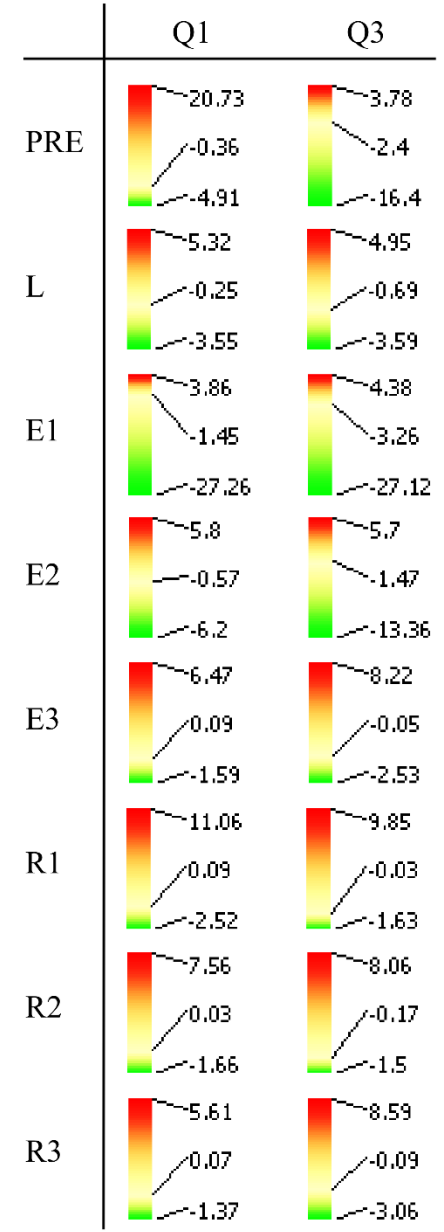
D 25% quantile	D 75% quantile	S segment	S well	S molecule_ID
0.954	1.146	R3	c1	control (1% DMSO)
0.301	0.699	R3	c10	N methyl D aspartic acid
0.477	0.903	R3	c11	control (1% DMSO)
0.602	0.778	R3	c12	amantadine
0.903	1.079	R3	c13	CGS 21680
0.602	0.845	R3	c14	ticlopidine
0.602	0.845	R3	c15	N methyl D aspartic acid
0.477	0.699	R3	c16	control (1% DMSO)
0.477	0.699	R3	c17	amantadine



**D**

Row ID	D (±)-U-50488-HCl	D BNTX maleate	D Etonitazenyl isothiocyanate
L_Q1	-1.375	-0.915	-1.453
L_Q3	-0.076	-0.415	-1.967
E1_Q1	-0.633	0.162	-2.651
E2_Q1	-0.23	1.15	-1.555
E3_Q1	0.101	0.047	0.052
IGNORE_Q1	-0.208	-0.118	-0.329
PRE_Q1	-0.375	0.098	-1.377
R1_Q1	-0.092	0.307	0.089
R2_Q1	-0.184	0.076	-0.134
R3_Q1	-0.089	0.124	-0.009
E1_Q3	-1.826	-1.229	-17.077
E2_Q3	-0.398	0.51	-2.912
E3_Q3	-0.276	-0.064	-0.428
IGNORE_Q3	-1.179	-0.83	-1.916
PRE_Q3	0.49	0.403	-4.188
R1_Q3	-0.325	0.636	-0.133
R2_Q3	-0.158	-0.233	-0.429
R3_Q3	-0.615	-0.104	-0.695

Figure 3

**A****Figure 4****B**

## Supplemental Materials

### A KNIME-based Analysis of the Zebrafish Photomotor Response Clusters the Phenotypes of 14 Classes of Neuroactive Molecules

*Daniëlle Copmans<sup>1</sup>, Thorsten Meinl<sup>2</sup>, Christian Dietz<sup>3</sup>, Matthijs van Leeuwen<sup>4</sup>, Julia Ortmann<sup>5</sup>,  
Michael R Berthold<sup>3</sup>, Peter AM de Witte<sup>1\*</sup>*

<sup>1</sup>Laboratory for Molecular Biodiscovery, Department of Pharmaceutical and Pharmacological Sciences, KU Leuven, Leuven, Belgium

<sup>2</sup>KNIME.com AG, Zurich, Switzerland

<sup>3</sup>Chair for Bioinformatics and Information Mining, Department of Computer and Information Science, University of Konstanz, Konstanz, Germany

<sup>4</sup>Machine Learning group, Department of Computer Science, KU Leuven, Leuven, Belgium

<sup>5</sup>Department of Bioanalytical Ecotoxicology, Helmholtz Centre for Environmental Research, UFZ, Leipzig, Germany

**\*Corresponding Author:**

Prof. Dr. Peter A. M. de Witte, Laboratory for Molecular Biodiscovery, Department of Pharmaceutical and Pharmacological Sciences, KU Leuven, Herestraat 49 bus 824, 3000 Leuven, Belgium.

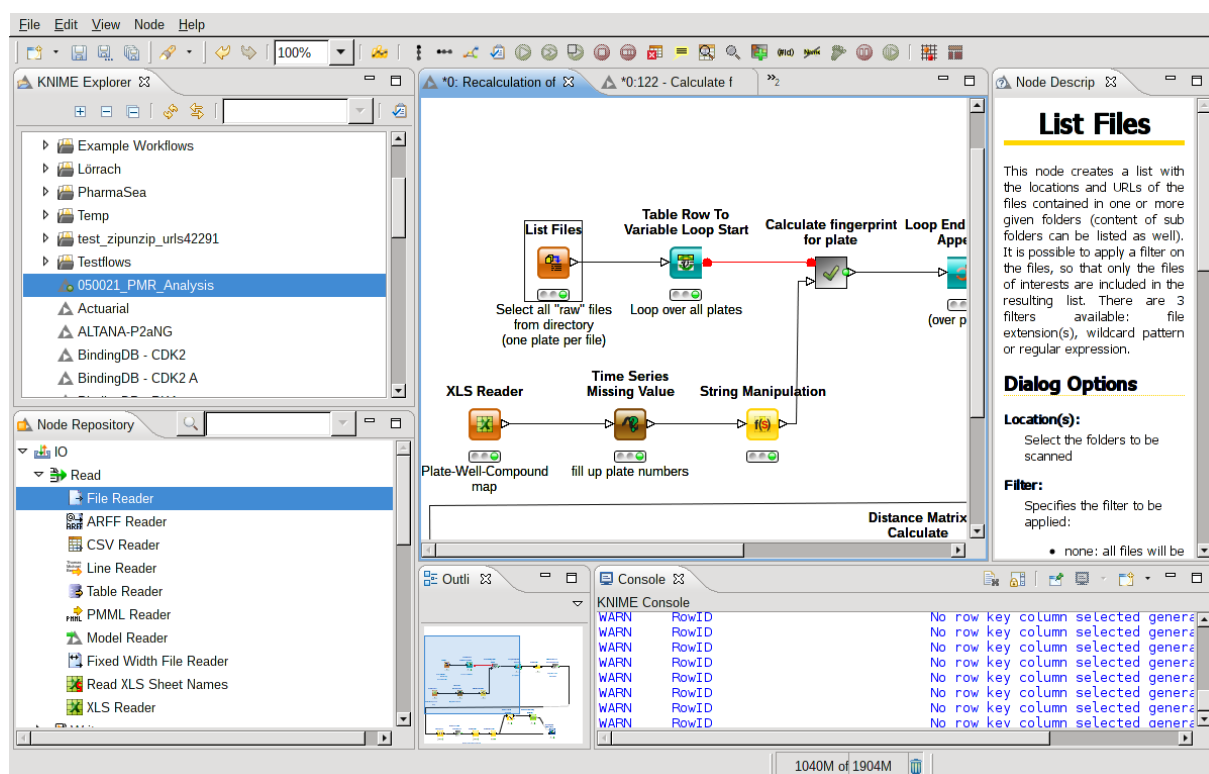
E-mail: peter.dewitte@pharm.kuleuven.be (P.A.M.W.)

## An automated KNIME workflow for large-scale PMR analysis

The KNIME workflow for PMR analysis is part of the supplemental material and can also be downloaded from the KNIME Public Example Server as 050\_Applications/050021\_PMR Analysis. The workflow requires at least KNIME Analytics Platform 2.11.1 with the following additional extensions:

- KNIME Math Expression (JEP)
- KNIME Nodes to create KNIME Quick Forms
- KNIME XLS Support
- KNIME JFreeChart
- HiTS experimental features (from <https://code.google.com/p/hits/wiki/Install>)

## KNIME Analytics Platform

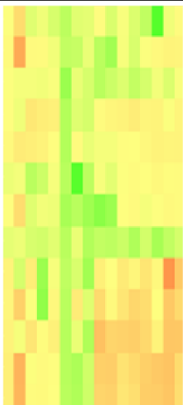
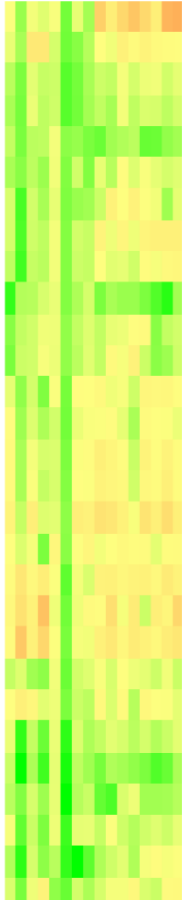


**Figure S1.** Screenshot of the KNIME Analytics Platform with an open workflow.

## Phenotypical clusters enriched with molecules from a single receptor class

Cluster	Behavioral fingerprint	Compound	Receptor class	Evaluation (N, S, or T)
1		Naltrindole HCl	opioid- ( $\delta$ )	N
		ICI 199,441 HCl	opioid+ ( $K$ )	N
		(-)-U-50488 HCl	opioid+ ( $K$ )	N
		Naltriben mesylate	opioid- ( $\delta$ )	N
		Tramadol HCl	opioid+ ( $\mu$ )	N
		( $\pm$ )-SKF-82958 HBr	DOPA+	N
		B-HT 920 2HCl	DOPA+	S
2		Neostigmine bromide	chol+	N
		8-Methoxy-2-propionamidotetralin	melat+	N
		Amthamine 2HBr	hist+	N
		Levallorphan tartrate	opioid $\pm$	N
		U-54494A HCl	opioid+	N
		(2S,4S)-4-Methylglutamic acid	mGlu+	N
		(1R,3R,4S)-1-Aminocyclopentane (1)	mGlu-	N
		(2S,1'S,2'R)-2-(Carboxycyclopropyl)glycine	mGlu+	N
		(RS)-4-Phosphonophenylglycine	mGlu+ (group III)	N
		GR 89696 fumarate	opioid+	N
3		WB 4101 HCl	A- ( $\alpha$ 1A)	N
		3-MPPI	A+ ( $\alpha$ 1)	N
		FGIN-1-27	GABA+	N
		FGIN-1-43	GABA+	N
		GR103691	DOPA-	N
		Terfenadine	hist-	N
		(1S,3R,4S)-1-Aminocyclopentane (1)	mGlu-	N
		8-(3-Chlorostyryl)caffeine	adenos-	N
		Fluorouracil	chol-	N
		Glyburide	K channel-	N
		Minoxidil sulfate	K channel+	N
		Cimaterol	A+ ( $\beta$ )	N
		O-Phospho-L-serine	mGlu+	N
		Isoproterenol HCl	A+ ( $\beta$ )	N
		Cabergoline	DOPA+	N
		Urapidil HCl	A- ( $\alpha$ 1)	N
		Clonidine HCl	A+ ( $\alpha$ 2)	N
		UK 14,304	A+ ( $\alpha$ 2)	N
		(D-ala2,N-me-phe4,glycol5)Enkephalin	opioid+	N
		Nalbuphine HCl dihydrate	opioid-,+	N
		Zilpaterol HCl	A+ ( $\beta$ )	N
		Guananz	A+ ( $\alpha$ 2)	N
		Rilmenidine hemifumarate	A+ ( $\alpha$ 2)	N

4		SIB 1893	mGlu- (mGlu5)	N
		2-Methyl-6-(phenylethynyl)pyridine HCl	mGlu- (mGlu5)	N
		PHCCC	mGlu- (group I)	S
		Fluspirilene	Ca and K channel-	N
		SIB 1757	mGlu- (mGlu5)	N
		3 <sup>7</sup> -Fluorobenzylpiperone maleate	DOPA-	S
		Haloperidol HCl	DOPA-	N
		Flufenamic acid	Na and K channel-	N
		NPPB	Cl channel-	N
		5		(+)-PD 128907
Piribedil 2HCl	DOPA+ (D3)			N
R(+)-6-BROMO-APB HBr	DOPA+ (D1)			N
Clomipramine	A+, 5-HT+			N
3α[(4chlorophenyl)phenylmethoxy]tropane HCl	DOPA+ (DRI)			N
Amitriptyline	A+, 5-HT+			N
GBR 12935 diHCl	DOPA+ (DRI)			N
S-eticlopride	DOPA- (D2)			T
6		Cyproheptadine HCl	5-HT-	T
		BP554 maleate	5-HT+	N
		Niguldipine	Ca channel-	S
		DH 97	melat-	T
		Amiodarone	Ca and Na channel-	T
		(±)-Epibatidine	chol+	S
		MDL-72222	5-HT-	N
		Propofol	GABA+	S
		Thapsigargin	iCa-	S
		NS-1619	K channel+	T
		2-(α-Naphthoyl)-ethyltrimethylammonium iodide	chol-	T
		5-Nonyloxytryptamine oxalate	5-HT+	T
		BRL 15572 HCl	5-HT-	N
		Clothiapine	DOPA-	N
		Ticlopidine HCl	purine-	N
		Dipropyldopamine HBr	DOPA+	N
		PRE-084 HCl	sigma-R+	N
		2,10,11-TrihydroxyNpropylnoraporphine HBr	DOPA+	S
		Clopidogrel sulfate	purine-	S
		Nicardipine HCl	Ca channel-	N
		Pimozide	Ca channel-	S
		7-Hydroxy-DPAT HBr	DOPA+	S
		GBR-12909 2HCl	DOPA+	N
		Aconitine	Na channel-	N
		FPL-64176	Ca channel+	N
		Nimodipine	Ca channel-	S
		Flunarizine 2HCl	Ca and Na channel-	S
		NNC 63-0532	opioid+	N
		SDZ-201106	Na channel+	N
		PCO-400	K channel+	N
		α-ERGOCRYPTINE	DOPA+	T
		Fluperlapine	5-HT+	N
Pizotifen maleate	5-HT-	N		

7		Cyproheptadine HCl	5-HT- (5-HT2)	T
		BP554 maleate	5-HT+ (5-HT1A)	N
		Niguldipine	Ca channel-	S
		DH 97	melat-	T
		Amiodarone	Ca and Na channel-	T
		(±)-Epibatidine	chol+	S
		MDL-72222	5-HT- (5-HT3)	N
		Propofol	GABA+	S
		Thapsigargin	iCa-	S
		NS-1619	K channel+	T
		2(α-Naphthoyl)ethyltrimethylammonium iodide	chol-	T
		5-Nonyloxytryptamine oxalate	5-HT+ (5-HT1B)	T
		BRL 15572 HCl	5-HT- (5-HT1D)	N
		8		Propyl-β-carboline-3-carboxylate
PNU 96415E	DOPA- (D4)			N
2Chloro11(4methylpiperazino)dibenz[B,F] (2)	DOPA- (D4)			S
L-741,742 HCl	DOPA- (D4)			S
Riluzole HCl	GABA+			T
Tolcapone	DOPA+ (COMT-I)			T
Ticlopidine	iGlu+			N
Nitrendipine	Ca channel-			N
SKF-96365	Ca channel-			N
N-phenylanthranilic acid	Cl channel-			N
Fipronil	Cl channel-, GABA-			N
Niflumic acid	Cl channel-			N
CL 218872	GABA+			S
L-750,667 3HCl	DOPA- (D4)			N
Loxapine succinate	DOPA- (D2, D4)			T
Trifluoperazine 2HCl	DOPA- (D2)			N
GBR 13069 2HCl	DOPA+ (DRI)			T
CGS 12066B dimaleate	5-HT+			N
Metergoline phenylmethyl ester	5-HT-			S
1-Allyl-3,7-dimethyl-8-phenylxanthine	adenos-			N
Mianserin HCl	5-HT-			N
Etonitazenyl isothiocyanate	opioid-			S
Methiothepin maleate	5-HT-			N
GBR 12783 2HCl	DOPA+ (DRI)			N
GBR 12935 2HCl	DOPA+ (DRI)			N
SKF-96365	Ca channel-			N
PD 168077 maleate	DOPA+ (D4)			N
Loratidine	hist-			T
PK-11195	GABA+			N

**Figure S2.** Detailed view of phenotypical clusters that are enriched with molecules from a single receptor class. A detailed view is given from clusters 1-8, indicated in the dendrogram from Figure 4. The cluster number is given in column 1. The behavioral fingerprint of each molecule within each cluster is given in column 2. The compound name is given in column 3. The receptor class of each compound is given in column 4, and the receptor/target of molecules that are enriched in a cluster is given between parentheses. The scores normal (N), sedative (S),

or toxic (T) which were given to each compound after microscopic evaluation of toxicity is given in column 5. (1), -1,3,4-tricarboxylic acid; (2), oxepin maleate;  $\delta$ , delta receptor; K, kappa receptor;  $\mu$ , mu receptor;  $\alpha$ ,  $\alpha$  receptor;  $\beta$ ,  $\beta$  receptor; DRI, dopamine reuptake inhibitor; COMT-I, catechol-O-methyl transferase inhibitor; DOPA, dopaminergic; chol, cholinergic; melat, melatonin; hist, histamine; mGlu, metabotropic glutamatergic; iGlu, ionotropic glutamatergic; A, adrenergic; GABA, GABAergic; adenos, adenosine; 5-HT, serotonergic; K, potassium; Ca, calcium; Na, sodium; Cl, chloride; iCa, intracellular calcium; +, agonist; -, antagonist;  $\pm$ , partial agonist.